scientific reports

Check for updates

OPEN

Establishment and genomic profiling of cholangiocarcinoma cells with functional characterization

Rattanaporn Jaidee[1,2], Apinya Jusakul[2,3], Piman Pocasap[1,2], Veerapol Kukongviriyapan[1,2], Laddawan Senggunprai[1,2], Auemduan Prawan[1,2], Watcharin Loilome[2,4], Attapol Titapun[2,5], Apiwat Jareanrat[2,5], Vasin Thanasukarn[2,5], Natcha Khuntikeo[2,5], Nisana Namwat[2,4], Yaovalux Chamgramol[6], Malinee Thanee[6], Phongsathorn Wichian[6], Jing Han Hong[7], Peiyong Guan[8], Hong Lee Heng[9], Chawalit Pairojkul[6], Bin Tean Teh[7,8,9,10] & Sarinya Kongpetch[1,2]✉

Cholangiocarcinoma (CCA) is a highly lethal hepatobiliary malignancy, with prognosis is influenced by anatomical subtypes and etiological factors. This study successfully established three CCA cell lines: KKU-097, KKU-466, and KKU-610, from the primary tumors of patients in liver fluke-endemic areas. These cells represent the perihilar CCA (pCCA) and intrahepatic CCA (iCCA) subtypes. Comprehensive analyses, including histopathology, molecular profiling, biomarkers, cancer phenotype characterization, and drug sensitivity testing with standard chemotherapeutics, were conducted. Whole-exome sequencing was performed to explore genetic alterations. All three cell lines exhibited adherent growth with an epithelial morphology and positive expression of the bile duct epithelial markers CK-7 and CK-19. Cytogenetic analysis revealed highly complex hypertriploid karyotypes with multiple chromosomal aberrations. Among the cell lines, KKU-610 demonstrated higher growth and invasion rates, whereas KKU-466 and KKU-097 cells exhibited less aggressive phenotypes. Drug sensitivity testing demonstrated relative resistance to gemcitabine as a monotherapy and in combination with cisplatin in all three cells. Genomic profiling identified targetable mutations, highlighting these new cell lines as valuable models for investigating the pathogenesis of CCA and evaluating therapeutic strategies.

Keywords Cholangiocarcinoma, CCA, *Opisthorchis viverrini*, Cell line, Liver fluke

Cholangiocarcinoma (CCA) is a highly lethal and heterogeneous group of hepatobiliary malignancies that arise from epithelial cells lining the biliary tree. Based on anatomical classification, CCA is categorized into intrahepatic CCA (iCCA) and extrahepatic CCA (eCCA), with the latter further subdivided into perihilar (pCCA) and distal CCA (dCCA)[1]. The incidence of iCCA has increased worldwide (0.3 to 6/100,000) and varies by geography. Certain regions, particularly, Thailand, Laos, Cambodia, South China, and Korea, report high incidences of CCA (more than 6/100,000)[2,3]. Liver fluke infection, particularly with *Opisthorchis viverrini* (*Ov*) and *Clonorchis sinensis* has been associated with carcinogenesis in some Southeast Asian countries. In contrast, in Western countries, primary sclerosing cholangitis (PSC) is the most common risk factor for CCA[4,5].

[1]Department of Pharmacology, Faculty of Medicine, Khon Kaen University, Khon Kaen, Thailand. [2]Cholangiocarcinoma Research Institute, Khon Kaen University, Khon Kaen, Thailand. [3]Centre for Research and Development of Medical Diagnostic Laboratories, Faculty of Associated Medical Sciences, Khon Kaen University, Khon Kaen, Thailand. [4]Department of Systems Biosciences and Computational Medicine, Faculty of Medicine, Khon Kaen University, Khon Kaen, Thailand. [5]Department of Surgery, Faculty of Medicine, Khon Kaen University, Khon Kaen, Thailand. [6]Department of Pathology, Faculty of Medicine, Khon Kaen University, Khon Kaen, Thailand. [7]Cancer and Stem Cell Biology Program, Duke-NUS Medical School, Singapore, Singapore. [8]Genome Institute of Singapore, Agency for Science, Technology and Research (A*STAR), Singapore, Singapore. [9]Laboratory of Cancer Epigenome, Division of Medical Science, National Cancer Center Singapore, Singapore, Singapore. [10]Institute of Molecular and Cell Biology, Agency for Science Technology and Research (A*STAR), Singapore, Singapore. ✉email: sarinyako@kku.ac.th

Over the past decade, high-throughput next-generation sequencing technology has unveiled genomic and epigenetic alterations in CCA, revealing that genomic heterogeneity is closely related to tumor location and underlying risk factors driving cholangiocarcinogenesis[6]. The mutational landscape differs between *Ov*-associated CCA and non-*Ov*-associated CCA. *Ov*-associated CCA exhibits high mutational frequencies in *TP53* and *ARID1A,* whereas non-*Ov*-associated CCA is characterized by high frequencies of mutations in *BAP1, IDH1/2,* and *FGFR2* fusions. Notably, *KRAS* mutations are common in both groups[7–9]. These findings suggest that actionable target genes may differ based on the etiology of CCA. This highlights the importance of patient-derived cell lines and organoids research tools for developing treatment strategies across different CCA subtypes.

Cancer cell lines are valuable tools for investigating the molecular mechanism of carcinogenesis and devising effective treatment strategies. Several patient-derived cell lines from CCA tumor tissues have been established, encompassing a range of gross pathological and histological subtypes. Approximately 75 CCA cell lines have been reported worldwide[10]. In northeast Thailand, where *Ov* infestation is endemic, we established cell lines, including KKU-100, KKU-213, KKU-023, and KKU-452 from CCA tumors collected from CCA patients[11–13]. Patient-derived CCA cell lines provide simple models yet representative the malignant characteristics of their tumor origin. To advance the understanding of CCA carcinogenesis and their distinct molecular and phenotypic characteristics, more CCA cell lines must be established as robust research tools for refining effective therapeutics for CCA treatment.

Results

Establishment of human CCA cell lines from surgical specimens

Three CCA cell lines were successfully established from pathologically proven CCA patients. The pathological profile and characteristics of the CCA patients are shown in Table 1. All patients were residence in the endemic area of liver fluke infection (*Ov*) in Northeast Thailand. Primary tumor tissues obtained during the surgical procedure from a 53-year-old female with pCCA were used to establish cultured cells and designated as KKU-097; cultured cells from a 62-year-old male with pCCA designated as KKU-466; and cultured cells from a 63-year-old female with iCCA designated as KKU-610 (Fig. 1A–C). A pathological analysis of the original tumor was conducted. H&E staining of KKU-097, KKU-466, and KKU-610 revealed that the cells were well-differentiated adenocarcinomas, intraductal papillary neoplasms of the bile duct (IPNB) with high-grade dysplasia, and poorly differentiated adenocarcinomas, respectively (Fig. 1D–F). Patient serum tumor marker levels were evaluated. The serum alpha-fetoprotein (AFP) levels of all patients were well within normal ranges, whereas most patients presented marked increases in carcinoembryonic antigen (CEA) and carbohydrate antigen 19-9 (CA 19-9) levels, with the exception of KKU-466, which presented normal CA 19-9 levels.

Morphological features of CCA cells

All new CCA cell lines grew as adherent monolayers. The cells were maintained in culture medium for more than 50 passages, indicating their stable genetics for long-term studies. KKU-097 and KKU-610 presented features of an irregular polygonal shape with multiple nuclei (Fig. 2A,C). KKU-466 had a smaller ovoid to cuboidal shape, forming a compact monolayer with multinuclear cells (Fig. 2B), suggesting its cellular heterogeneity. Immunocytochemical staining for the cholangiocyte markers CK-7 and CK-19 was positive in all the cell lines, suggesting that they originated from the bile duct epithelium (Fig. 2D–I). Mycoplasmas were not detected in the culture medium during the series of experiments. All the cell lines could be propagated under cryopreservation with no change in the characteristics of the cells at different passages.

Patient characteristics	KKU-097	KKU-466	KKU-610
Age (years)	53	62	63
Sex	Female	Male	Female
Survival after surgery (days)	277	1427	158
Gross pathology	pCCA, mass-forming type at hilar of the liver	pCCA, intraductal growing type of left hepatic duct	iCCA, mass-forming type at segment III of left lobe
Histopathology	Well-differentiated adenocarcinoma	IPNB with high grade dysplasia	Poorly differentiated adenocarcinoma
Serum AFP (0.0–10.0 IU/mL)[a]	8.82	3.21	4.67
Serum CEA (0.0–2.5 ng/mL)[a]	7.99	5.50	69.0
Serum CA 19–9 (0.0–37.0 U/mL)[a]	> 1000	< 0.6	> 1000
Cell line characteristics	**KKU-097**	**KKU-466**	**KKU-610**
Origin	Primary tumor	Primary tumor	Primary tumor
Growth characteristics	Adherent	Adherent	Adherent
Doubling time	32 h	56 h	27 h
Immunocytochemistry CK-7[b]	+ + +	+ +	+ + +
Immunocytochemistry CK-19[b]	+ + +	+ +	+ + +

Table 1. Pathology profile of CCA patients and characteristics of established cell lines. [a]Reference value. [b]ICC Grading: − = negative, + = < 25% tumor cell stained, + + = 25–50% tumor cell stained, + + + = > 50% tumor cell stained.

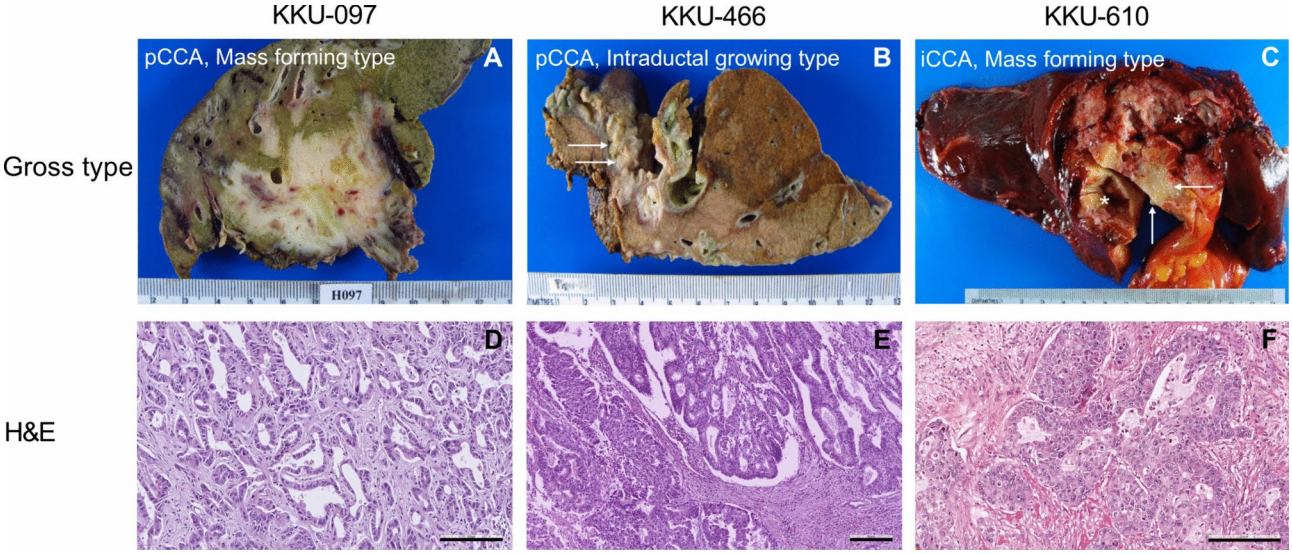

Fig. 1. Gross pathology and histopathology of the original tumors. (**A**–**C**) Gross pathology of the surgically resected specimen showing pCCA (KKU-097 and KKU-466) and iCCA (KKU-610). The arrows highlight the tumor parenchyma, and the asterisks indicate artifacts and sampling artifacts. (**D**–**F**) H&E staining revealed histopathology of KKU-097 cells with IPNB with high-grade dysplasia, KKU-466 cells with poorly differentiated adenocarcinoma, and KKU-610 cells with well-differentiated adenocarcinoma (scale bar = 200 μm).

Karyotype and short tandem repeat (STR) profiles of CCA cell lines

Newly generated CCA cells were subjected to karyotype analysis. Numerical and structural aberrations were found in all the cell lines. KKU-097 cells were characterized as hypertriploid with a modal chromosome number of 74 (near-triploidy, 69±). The pattern of numerical abnormalities included nullisomy 22, monosomy 21, trisomy 1, 2, 3, 6, 8, 11, 13, and 17 and tetrasomy 9, 15, 16, and X. For structural abnormalities, the pattern included deletions of chromosomes 7q22, 7q32, and 10q22 and additional chromosomes of 12q24.3 and 14q32 (Fig. 3A). The KKU-466 cell line was a hypertriploid cell line with a modal chromosome number of 76, occurring in 20% of the cells. Monosomy 13 and iso(1)(p10p10) were present in all metaphases. Most cells had two X chromosomes (Fig. 3B). KKU-610 was a hypertriploid cell line with 70 modal chromosomes (near-triploidy, 69±). Trisomy 2, 4, 5, 10, 15, and 21; tetrasomy 11 and 12; and 3; and pentasomy 20 and X were presented. Structural alterations included the translocation of chromosomes 1q32 and 3p23, the translocations of 8q24.3 and 17p13, the additional chromosomes 1q25 and 13q10, and the isochromosomes of 14p10 and 17q10 (Fig. 3C).

The STR profiles (24 loci) of the KKU-097, KKU-466, and KKU-610 cell lines from the two sources, the CCA cell lines and their original tissues, were analyzed to determine the identity of the cell lines. In the assessment of STR profiles, KKU-097 exhibited 88% similarity to the original tumor tissue across 24 loci, whereas KKU-610 displayed 70% concordance. Notably, while some loci demonstrated only one missing allele compared with the original tissue, others exhibited consistent allele retention (Supplementary Table S1). These findings indicate the presence of genetic heterogeneity of tumor tissues or genetic instability during the establishment of the cell lines. For KKU-466, although no tissue match was available, its STR profile was distinct and non-overlapping with KKU-097 and KKU-610, confirming its unique identity as a model for pCCA.

Cell growth, migration, and invasion analysis

The three cell lines presented different growth rates, with doubling times of 32 h, 56 h, and 27 h for KKU-097, KKU-466, and KKU-610, respectively (Table 1, Fig. 4A). All the cell lines formed colonies, as shown by the clonogenic assay (Fig. 4B). The migration potential of CCA cells was evaluated via a wound healing and transwell migration assay. KKU-610 cells highly migrated by closing the scratch wound within 18 h. Meanwhile, the scratch wounds of KKU-466 and KKU-097 cells were closed after incubation for approximately 72 h and more, respectively (Fig. 4C–H). Similarly, in the transwell migration assay, KKU-610 cells exhibited a very high migratory capability, completing migration within 24 h. KKU-097 cells showed a moderate migration rate, while KKU-466 cells displayed the lowest migratory activity (Fig. 4I). Consistent with their ability to migrate, KKU-610 cells exhibited a high invasion rate. In contrast, a much lower degree of invasion was observed with KKU-466 and KKU-097 (Fig. 4J). These data suggest the highly aggressive ability of KKU-610 cells.

Sensitivity to standard chemotherapy

The combination of gemcitabine (Gem) and cisplatin (Cis), the current first-line chemotherapeutic drug for patients with advanced CCA[14,15] was evaluated for the sensitivity in new CCA cells. The cells were treated with 0–25 μM Gem or 0–100 μM Cis for 24, 48, or 72 h. KKU-097 and KKU-610 cells were responsive toward Cis cytotoxicity, with the maximum killing (Emax) reaching nearly 100% in a concentration- and time-dependent

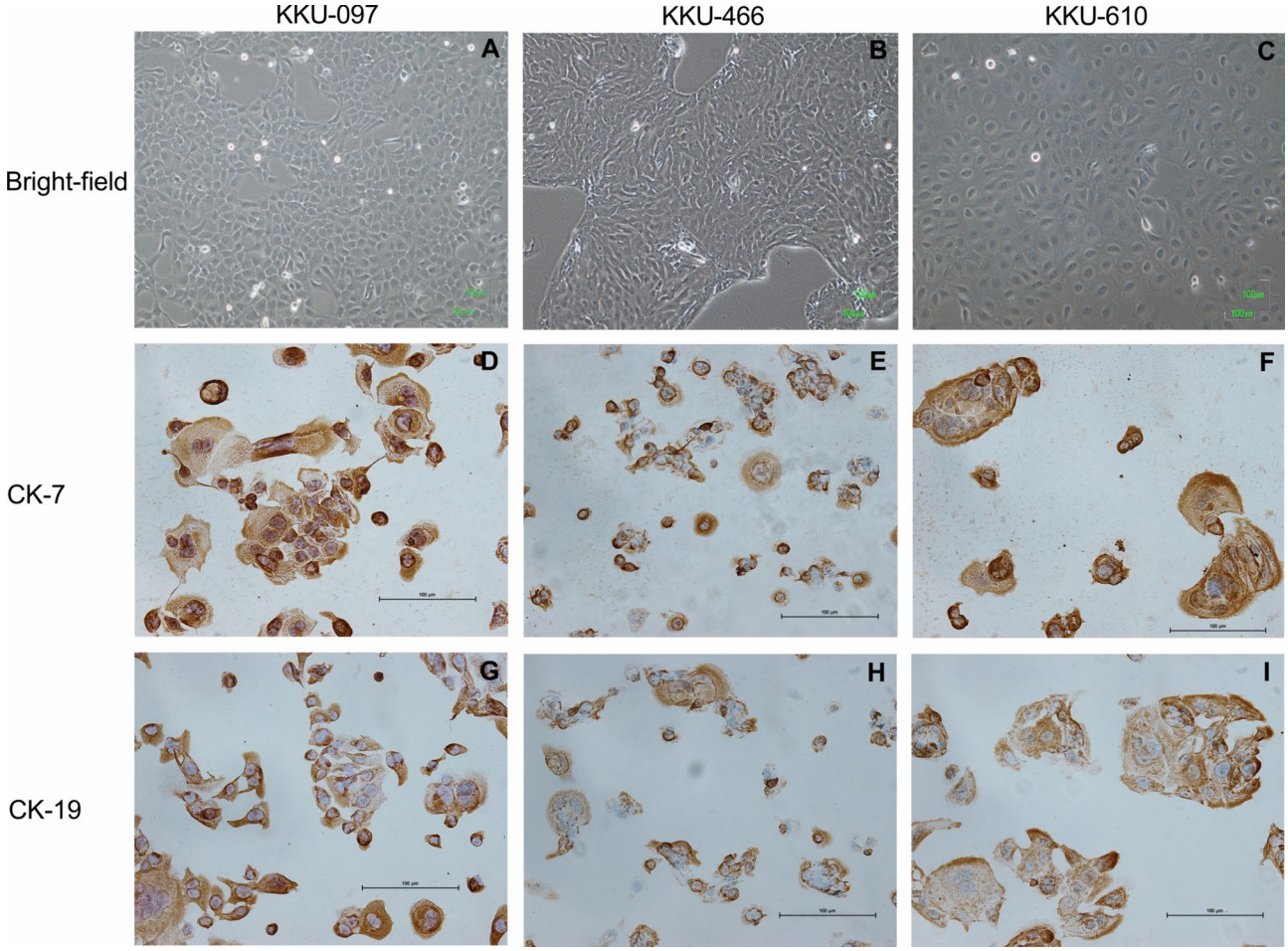

Fig. 2. Morphology and immunocytochemistry of CK-7 and CK-19 in CCA cells. (**A**–**C**) Phase-contrast microscopy was used to observe the brightfield morphology of KKU-466, KKU-610, and KKU-097 cells in the 45th, 60th, and 66th passages (10X magnification, scale bar = 100 μM). (**D**–**I**) Immunocytochemistry of CK-7 and CK-19. All CCA cells were cultured in slide chambers for 24 h, and the cells were fixed and stained with CK-7 and CK-19 antibodies (20X magnification, scale bar = 100 μM).

manner. In contrast, KKU-466 cells were much less responsive (Fig. 5A–C,G). On the other hand, Gem showed low efficacy toward the CCA cells, as the estimated Emax values were less than 50% at the highest concentration of Gem (25 μM). However, the IC50 values were calculated for further experiments (Fig. 5D–G).

To evaluate the effects of the interaction of the two drugs on cytotoxicity, various concentrations of Gem and Cis at around the IC50 values or lower for each drug were combined for 72 h. When these drugs were used in combination, the combination did not increase cell killing by more than 50%, as shown in the 3D surface plots (Fig. 5H–J). The interactive effects of the drug combinations assessed by the Bliss synergy score revealed that most Gem/Cis combinations resulted in Bliss scores ranging from 0 to −20, indicating additive to antagonistic effects (Fig. 5K–M). These findings suggested that all the new CCA cell lines were insensitive to the combination of Gem and Cis.

Comprehensive genomic sequencing of CCA cell lines

Whole-exome sequencing (WES) was used to analyze gene mutations in 6 CCA cell lines, including KKU-097, KKU-466, KKU-610, and three previously established cell lines, namely, KKU-023, KKU-100, and KKU-452[11,12]. Among these, original tumor tissues for establishing four cell lines: KKU-023, KKU-097, KKU-452, and KKU-610, were available for genetic comparison. We found that the CCA cells harbored mutations in genes involved in CCA pathogenesis, including genes related to genome instability (e.g., *TP53, BARD1, MSH3*), epigenetic modifiers (e.g., *ARID1A, KMT2C, IDH1*), DNA damage and cell cycle control (e.g., *BRCA1, CDKN1B, SMAD4*), kinase RAS/RAF (e.g., *KRAS, PIK3CA*), and WNT signaling (e.g., *AFF4, CTNNB1*). We then investigated whether the characteristics of the original tissues were preserved in the cell lines. The established cell lines maintained the mutations identified in the corresponding original tissues at the same position in the six most recurrent mutated genes: *TP53*, *KRAS*, *SMAD4*, *ARID1A*, *PIK3CA*, and *NCOR1* (Fig. 6A and Supplementary Table S2–S3). Notably, the KKU-023 cell line presented the highest number of somatic mutations concordant with its original tissue (Fig. 6A).

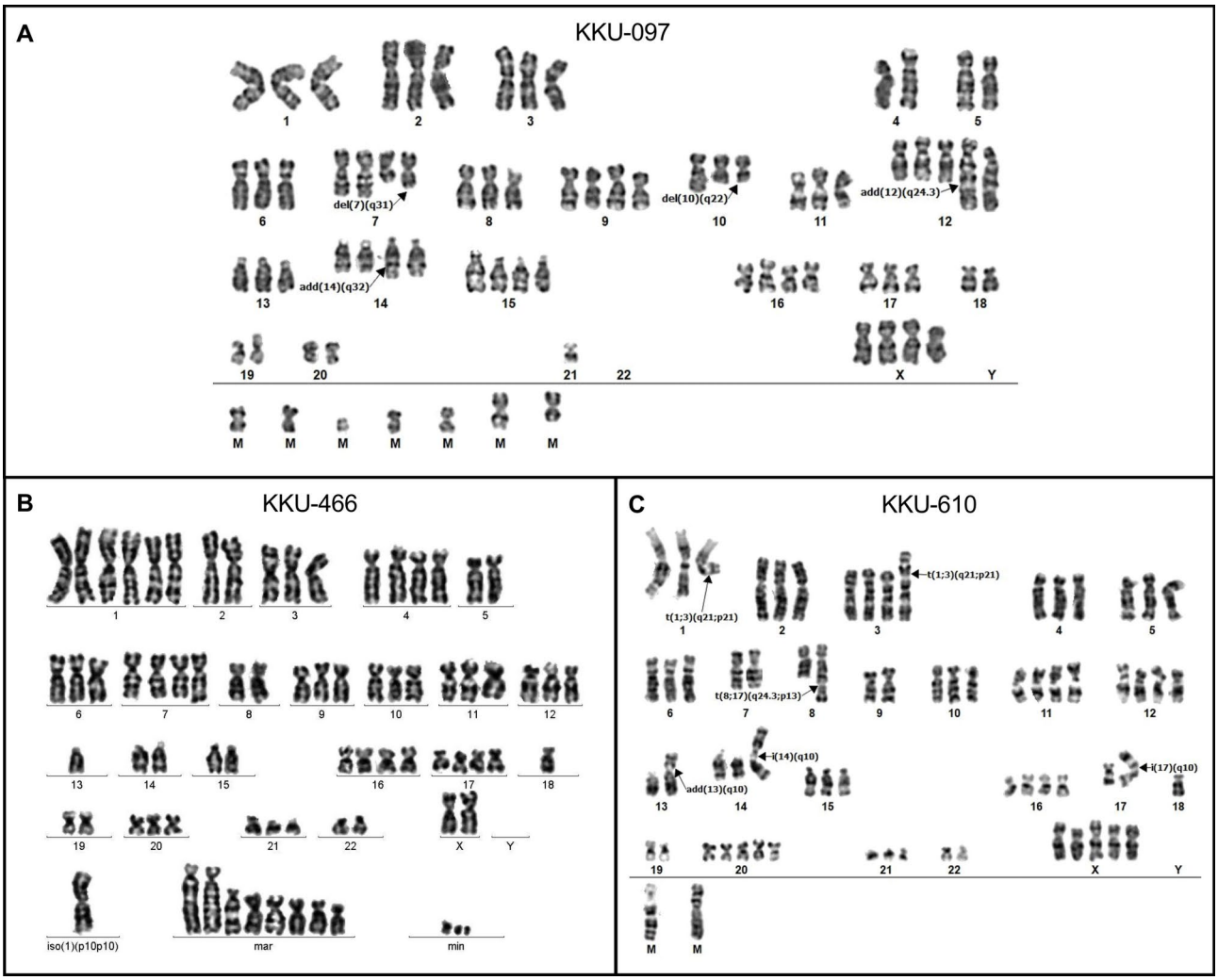

Fig. 3. Representative karyotypes of CCA cell lines. (**A**) The karyotype of the KKU-097 strain was 74 < 3n > ,XXX, + X, − 4,5,del(7)(q22), + del(7)(q31), + 9,del(10)(q22), del(10)(q22), add(12)(q24.3), + add(12)(q24.3),add(14)(q32), + add(14)(q32), + 15, + 16, − 18, − 19, − 20, − 21, − 21, − 22, − 22, − 22, + 7mar. (**B**) KKU-466 cells were 76,XX, + 1, + 3, + 4, + 6, + 7, + 9, + 10, + 11, + 12, − 13, + 16, + 17,18, + 20, + 21 + iso(1)(p10p10), + mar, + min. (**C**) KKU-610 showed 70 < 3n > ,XXX, + X, + X, add(1)(q25),der(1)t(1;3)(q32;p23), + der(3)t(1;3)(q32;p23), − 7, − 8,der(8)t(8;17)(q24.3;p13), − 9, + 11, + 12, − 13,add(13)(q10),i(14)(p10), + 16, − 17,i(17)(q10), − 18, − 18, − 19, + 20, + 20, − 21, − 22, + 3mar.

Moreover, these established CCA cell lines presented many targetable mutations with preclinical and clinical evidence. According to the OncoKB database, a total of five actionable mutations were identified. KKU-023 harbored an actionable mutation in *PIK3CA*^{H1047R} and *ATR*^{I774Nfs*3} (therapeutic level of evidence 1) and *ARID1A*^{D1850Gfs*4} mutations (level of evidence 4). KKU-466, KKU-100, KKU-097, and KKU-452 harbored mutations in *PIK3CA*^{R88Q} (level 1), *KRAS*^{G12D} (level 3), *KRAS*^{G13C} (level 4), and *ARID1A*^{N1571*} (level 4), respectively. *BRCA1* genes found in KKU-023, KKU-097, and KKU-610 were assigned as likely oncogenic genes. For those genes, annotated alterations of *BRCA1*, *ATR*, and *ARID1A* were truncating mutations, suggesting loss of function, whereas *PIK3CA* and *KRAS* were missense mutations (Fig. 6B and Supplementary Table S2).

TP53 and *KRAS* mutations are the most common mutated genes in CCA pathogenesis. We further evaluated and confirmed the mutation of these two genes in all new cell lines by using Sanger sequencing. KKU-100 was used as a reference cell line with *KRAS* and *TP53* mutations[11]. In the *TP53* mutation analysis, KKU-100, KKU-466, and KKU-097 cells presented missense mutations. Moreover, KKU-466 contained insertion nucleotide bases affecting the DNA-binding domain, leading to a frameshift mutation, and KKU-610 cells presented a truncating mutation. *KRAS* oncogenic mutations were identified in 33.3% (2/6) of our established cells. KKU-097 cells presented a missense mutation at codon G13C, a position different from that of KKU-100, which was mutated at codon G12D in exon 2 (Fig. 6C,D). This result was consistent with the WES analysis.

A large set of CCA cells was recruited in principle component analysis of mutational variations to explore the heterogeneity of CCA cells. Notably, mutations in *KRAS*, *PIK3R1*, and *FANCD2* were associated with the CCA cells, including KKU-100, KKU-055, KKU-213A, KKU-213B, and KKU-213C cells. While *PTEN*, *STK11P*, *EGF*,

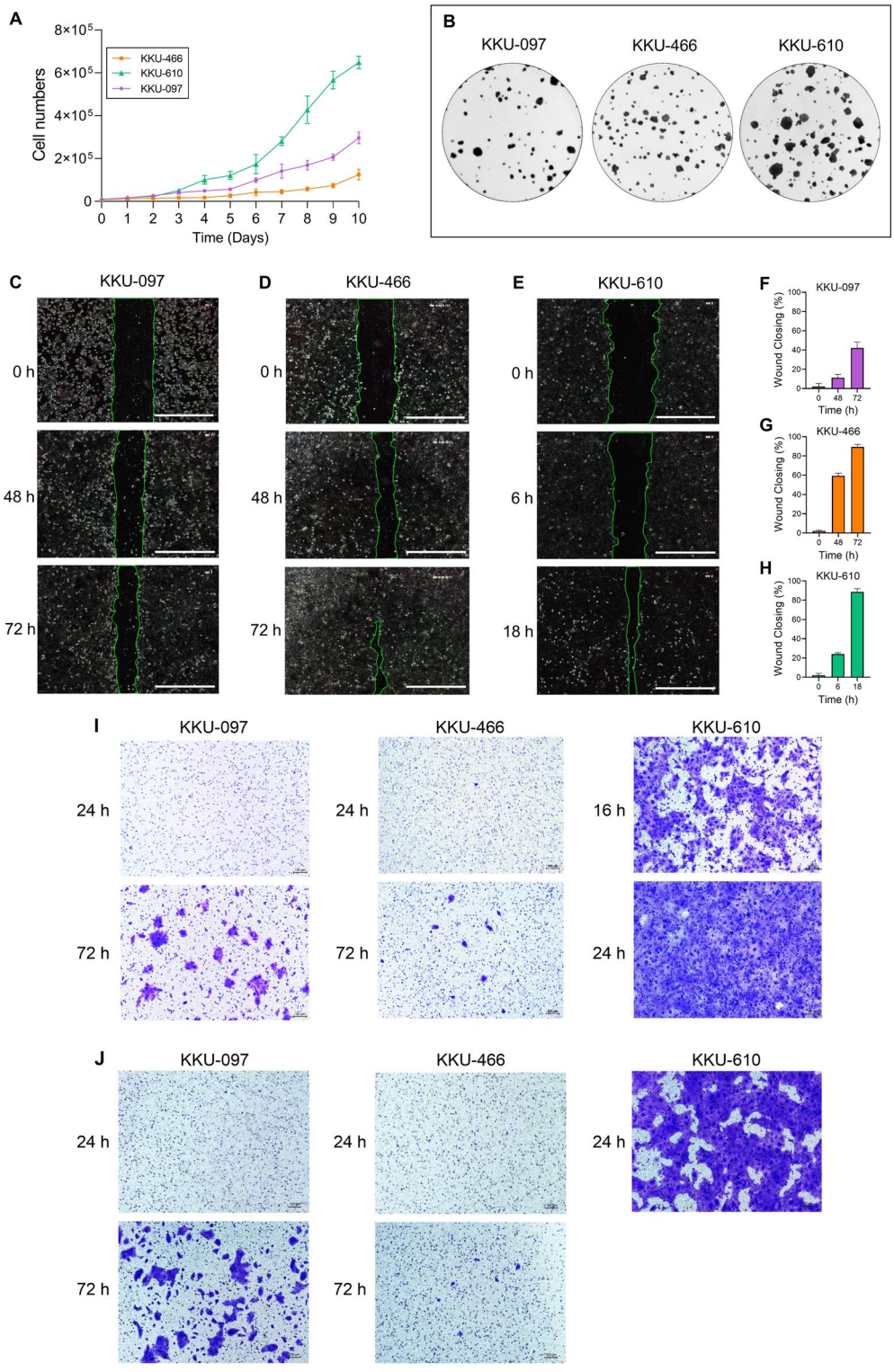

Fig. 4. Characterization of CCA cell lines. (**A**) Growth curve of CCA cells. (**B**) Representative images of the colony formation ability of each cell line. (**C**–**E**) Representative images of CCA cell migration were captured at 4X magnification (scale bar = 1000 μM). CCA cells were seeded onto 24-well plates. After the cells formed a confluent monolayer, a scratch line was made, and the distance of the scratch wound was measured after incubation until the wound closed. (**F**–**H**) Each bar represents the mean ± SD of wound closure. (**I**) Representative transwell migration and (**J**) invasion assay images were captured at 10X magnification (scale bar = 100 μM). For the migration assay, CCA cells were seeded in serum-free medium onto uncoated Transwell inserts. For the invasion assay, CCA cells were seeded onto Matrigel-coated Transwell inserts and incubated for 24 or 72 h. After incubation migrated and invaded cells were fixed, stained, and photographed.

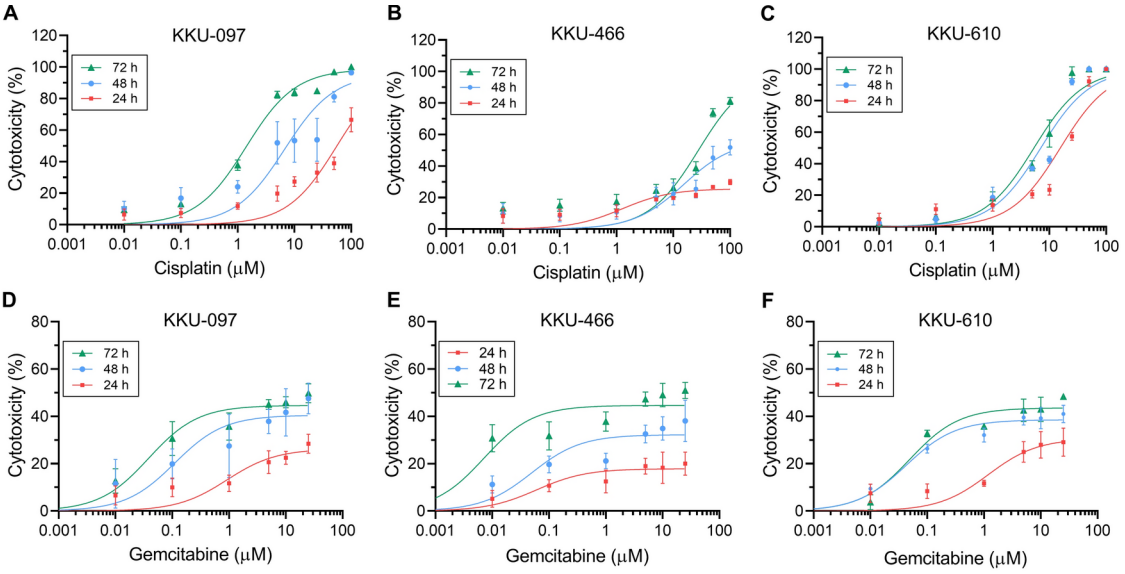

G

		KKU-097		KKU-466		KKU-610	
	Time	IC_{50} (μM)	Emax (%)	IC_{50} (μM)	Emax (%)	IC_{50} (μM)	Emax (%)
Cisplatin	24 h	56.1 ± 10.2	100 ± 5.6	22.1 ± 8.3	46.4 ± 4.3	15.6 ± 2.8	~100
	48 h	6.7 ± 1.6	95.6 ± 4.3	52.6 ± 10.6	90.3 ± 5.7	7.1 ± 1.1	~100
	72 h	1.4 ± 0.2	98.7 ± 1.4	25.8 ± 4.6	100 ± 4.6	5.4 ± 0.7	~100
Gemcitabine	24 h	0.920 ± 0.475	26.3 ± 2.5	0.060 ± 0.034	17. 9 ± 1.3	1.185 ± 0.525	30.6 ± 2.7
	48 h	0.111 ± 0.058	40.5 ± 3.0	0.050 ± 0.024	32.3 ± 2.0	0.043 ± 0.010	38.5 ± 1.1
	72 h	0.039 ± 0.111	44.6 ± 1.6	0.007 ± 0.003	44.6 ± 2.0	0.049 ± 0.012	43.6 ± 1.4

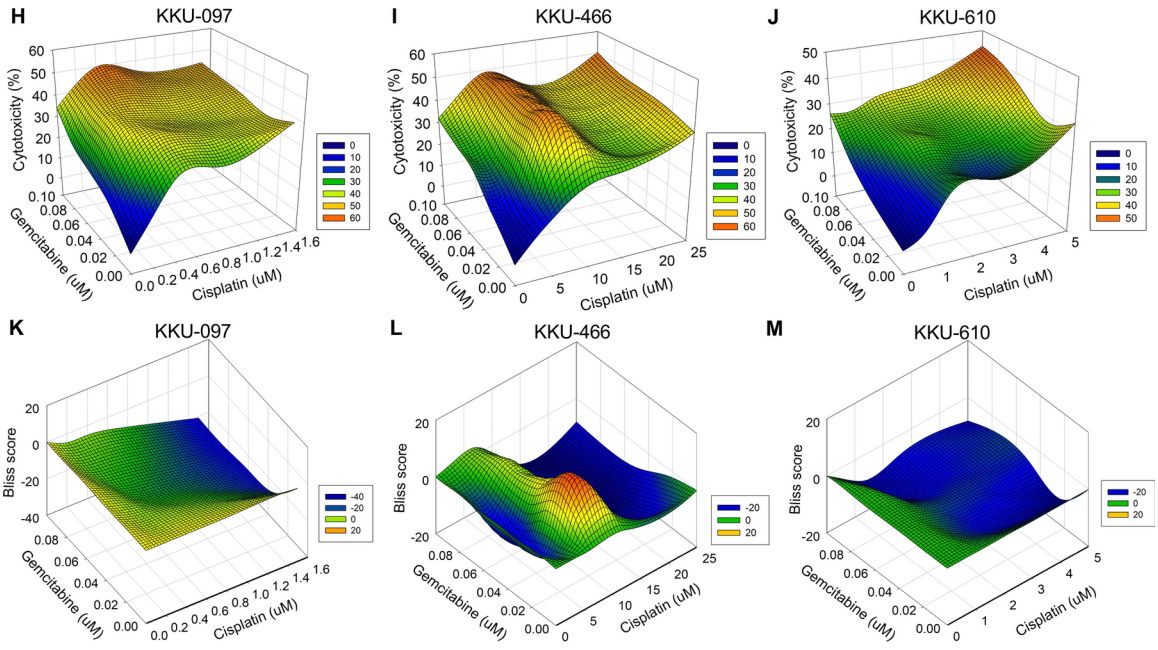

Fig. 5. Relative cytotoxicity of chemotherapeutic drugs in CCA cell lines. (**A**–**F**) Sensitivity of CCA cells to cisplatin (Cis) and gemcitabine (Gem). The cells were treated with Gem or Cis for 24, 48, or 72 h. Cell cytotoxicity was assessed via the MTT assay. Dose–response curves are expressed as the mean ± SD of three independent experiments. (**G**) The IC50 values of single drug treatment at 24, 48, and 72 h are shown. (**H**–**J**) The cytotoxicities of Gem, Cis, and the combination of Gem and Cis at concentrations up to their IC50 values at 72 h were determined via the MTT assay. (**K**–**M**) Drug synergism analysis was performed via a two-agent model in which the Bliss score was compared.

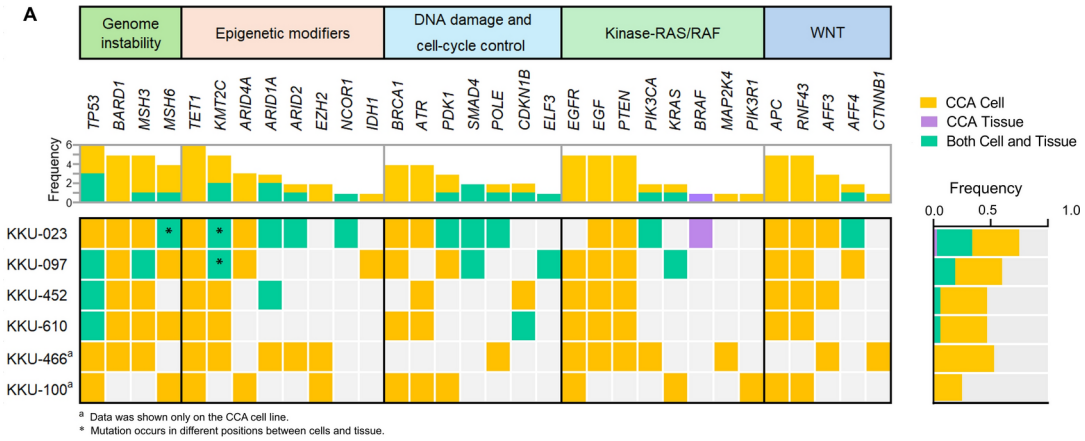

B

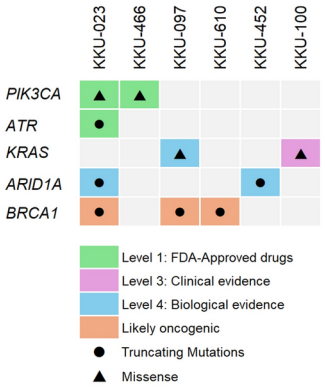

C

Sample	cDNA Annotation	Protein Annotation	Mutation
KKU-100	*TP53* c.215 C>G	TP53 p.P72R	Missense
KKU-466	*TP53* c.166 ins GTTCACTA	TP53 fs	Frameshift
KKU-466	*TP53* c.215 C>G	TP53 p.P72R	Missense
KKU-610	*TP53* c.1006 G>T	TP53 p.E366*	Nonsense
KKU-097	*TP53* c.215 C>G	TP53 p.P72R	Missense

Sample	cDNA Annotation	Protein Annotation	Mutation
KKU-100	*KRAS* c.35 G>A	KRAS p.G12D	Missense
KKU-466	*KRAS* WT	KRAS WT	-
KKU-610	*KRAS* WT	KRAS WT	-
KKU-097	*KRAS* c.37 G>T	KRAS p.G13C	Missense

D

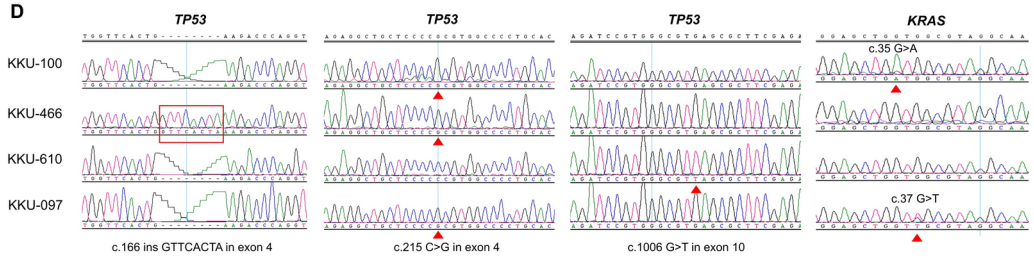

E

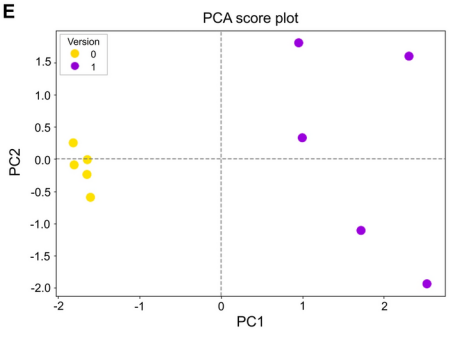

F

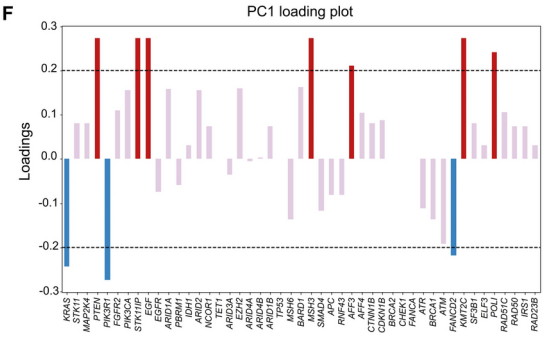

MSH3, *AFF3*, *KMT2C*, and *POLI* were observed in the group of CCA cells including KKU-097, KKU-466, KKU-610, KKU-023 and KKU-452 cells (Fig. 6E,F).

Discussion

CCA is the second most common hepatobiliary malignancy and is characterized by a very poor prognosis and limited treatment options[2,4]. The evidence indicates that CCA is heterogeneously associated with various etiologies. Our previously published data demonstrated that genetic alterations in *Ov*-associated CCA differ from those in non-*Ov*-associated CCA[9,16]. Establishing more cell lines with diverse genetic variations can reveal the heterogeneity of human tumors, facilitating a comprehensive investigation into the complex molecular pathways underlying cancer progression, vulnerability pathways, and translational research.

◀**Fig. 6**. Genomic sequencing of CCA cell lines (**A**) Comparison of mutations identified in CCA cells and their original samples. Genes harboring mutations were classified into 5 categories: genome instability, epigenetic modifiers, DNA damage and cell cycle control, kinase RAS/RAF, and WNT signaling. Frequencies of mutations identified as tissue-specific, CCA cell-specific, or both cell- and tissue-specific. (**B**) Coding variants with preclinical or clinical evidence of treatment according to the OncoKb database (May 23rd, 2024). Each column represents a cell line. Green: Level 1; Pink: Level 3; Light Blue: Level 4; Orange: Likely pathogenic. The symbols are as follows: circle, truncating mutation; triangle, missense mutation. (**C**) Annotated alterations in *TP53* and *KRAS* were detected in CCA cell lines. (**D**) A representative image of the sequencing traces of amplified *TP53* (NM_000546) and *KRAS* (NM_004985) in the KKU-100, KKU-466, KKU-610, and KKU-097 cell lines is shown. The red triangle and square represent point mutation and nucleotide insertion, respectively. (**E**) Principal component analysis (PCA) score plot of the mutational spectrum data showing the separation between the older set (yellow dots) and the new set (purple dots) of established CCA cell lines. (**F**) PCA loading plot highlighting the gene set contributing to the PC1 loading variable. The blue bars indicate the gene set contributing to the negative loading, which correlates with the older group of CCA cell lines; the red bars indicate the gene set contributing to the positive loading, which is associated with the newly established group of CCA cell lines.

This study successfully established three new CCA cell lines, KKU-097, KKU-466, and KKU-610, derived from three CCA patients. These cell lines were genetically profiling via STR analysis and found to be concordant with primary tumor tissues. Characterization included chromosome analysis, determinations of doubling time, migration and invasion ability, drug sensitivity, and comprehensive genomic profiling.

AFP and CA 19-9 are circulating tumor markers associated with hepatocellular carcinoma (HCC) and CCA, respectively, whereas CEA is a marker for CCA and many malignant tumors[17–19]. Increased levels of CA 19-9 and CEA were observed in all new CCA cell lines, except KKU-466, which presented normal CA 19-9 levels. However, the AFP level remained within the normal range. The growth kinetics of the three cell lines were correlated with the survival time of patients, with KKU-466 showing a slow growth rate, which is consistent with the very long survival time of the patient ($r = 0.99$, $p = 0.049$) from whom this cell line was developed.

Karyotyping analysis revealed numerical and structural abnormalities, including monosomy, trisomy, and tetrasomy, across various chromosomes in all new cell lines. These chromosomal aberrations contribute to CCA pathogenesis and influence tumor behavior and the response to chemotherapeutic agents. For example, a hypertriploid or near-triploid karyotype, identified as a hallmark of aggressive cancer behavior, chemotherapy resistance, and poor prognosis[20], was observed in all CCA cell lines with modal chromosome numbers ranging from 70 to 76. Previous research has reported that breast cancer cells with near-triploid karyotypes are resistant to paclitaxel and doxorubicin due to DNA damage mechanisms and increased Ki67 expression[21].

Migration and invasion are critical processes in cancer metastasis[22,23]. Understanding their underlying mechanisms is crucial for targeting and inhibiting cancer progression. In our study, KKU-610 cells exhibited highly aggressive behavior, characterized by high migration and invasion rates, followed by KKU-097 cells. The high aggressiveness of KKU-610 cells may be attributed to their histopathological classification as poorly differentiated adenocarcinoma. Conversely, KKU-466 cells demonstrated a less metastatic phenotype, were derived from intraductal papillary neoplasm of the bile ducts (IPNB), a histology type associated with a generally good prognosis [24,25].

The Gem/Cis regimen is the standard of care for patients with unresectable or metastatic CCA[14,15]. Despite its clinical efficacy, the overall survival of patients remains unsatisfactory. In cisplatin study, KKU-097 cells appeared to be the most sensitive, whereas KKU-466 cells were the least sensitive. The IC50 value and Emax of KKU-097 are comparable to those of KKU-055, another CCA cell line. For Gem, all three cells have very limited efficacy, as the Emax was less than 50%, similar to KKU-055 cells, which demonstrated Emax of approximately 50%[26]. Moreover, other cells derived from iCCA, including RBE, ICC-X1, and ICC-X2 cells, are relatively resistant to Gem[27,28]. The present study investigated whether a combination of Gem and Cis could improve the efficacy of cell killing in these three resistant cell lines. The overall effect of the combined drugs of Gem/Cis was unsatisfactory. Some combinations even showed antagonistic effects by decrease of cytotoxicity. Resistance to Gem may be an innate resistance mechanism, increasing the ability to repair drug-induced DNA alterations or overactivation of an oncogenic signaling pathway. The present study highlights the limited efficacy of current Gem/Cis treatments, which results in a poor therapeutic response[29]. These findings suggest that novel chemotherapy strategies are needed to achieve an optimal therapeutic response. Furthermore, genetic alterations such as *ARID1A* mutation, *PTEN* deficiency, and *BAP1* deficiency, especially SNPs in *PTEN*, contribute to Gem-based chemotherapeutic response in CCA[30–32]. Therefore, understanding genetic alterations is essential for predicting chemotherapeutic responses and providing therapeutic options for chemoresistant CCA patients.

It was well-documented that the pathogenesis of CCA was different depending on geographical regions and etiological factors, including liver fluke infestation. Our limitation of samples, only 6 CCA cell lines, may not reflect the whole subsets of CCA. However, our result revealed a mutational pattern consistent with *Ov*-associated CCAs characterized by mutations enriched in *ARID1A*, *KRAS*, and *TP53*. In contrast, *BAP1* and *FGFRs* alterations were more frequently found in non–*Ov* associated CCA[1,2], but was not detected in our newly established cell lines. This suggested our established CCA cells reflected the different etiological factors regarding the pathogenesis of CCA[7]. Long-term culture of cells as 2D monolayers can lead to the acquisition of additional mutations, which is a limitation of our study. However, to provide the relevance of the cell lines, we compared their genomic profiles with those of the original tumor tissues. We identified common mutated genes of CCA

in both the cell lines and matched tumor tissues, including *TP53*, *KRAS*, and *ARID1A*. These shared mutations support the validity of using these cell lines as models for CCA research.

In this study, six established CCA cell lines, three cells from the present study and another three cells from previous studies, presented many targetable mutations with preclinical and clinical evidence. At least five actionable mutations (*ARID1A, BRCA1, PIK3CA, KRAS,* and *ATR* mutations) were identified. *ARID1A* genes usually have inactive mutations that render *ARID1A* loss of expression[33,34], our KKU-023 and KKU-452 cell lines also harbor truncating mutations in *ARID1A*. Various treatment regimens targeting *ARID1A* mutations are in phase II clinical trials[35]. *KRAS* is one of the most common oncogenic genes in cancer, and many efforts have been made to develop covalent allele-specific inhibitors that trap $KRAS^{G12C}$ in its inactive conformation[36] and effectively in suppressing tumor growth in cancer patients[37,38]. At least two KRAS inhibitors have been approved by the U.S. FDA, with several others in clinical trials[39]. Our cell lines harboring *KRAS* mutants may be valuable tools for developing *KRAS*-directed therapeutics, particularly in *KRAS*-driven CCA. *BRCA1* is a tumor suppressor gene involved in DNA damage repair (DDR) via homologous recombination. Dysfunction of *BRCA* causes genomic instability, promoting tumor progression[40]. Previous studies demonstrated synthetic lethality between *BRCA* gene defects and DDR inhibition, leading to increased double-strand breaks and cancer cell death[41]. *BRCA*-deficient tumors exhibit high sensitivity to DDR inhibitors due to synthetic lethality mechanisms. Several PARP inhibitors (olaparib, niraparib, talazoparib, and rucaparib) have been approved for treating *BRCA*-mutant cancers[42]. KKU-023, KKU-610, and KKU-097 represent *BRCA1* truncation mutations, which are valuable for researching and developing new targeted drugs for a subgroup of CCAs. Interestingly, comutations in *KRAS* and *TP53,* which are observed in KKU-097 cells, are linked to DDR deficiency, leading to an increased mutation load in cancer cells[43]. Targeting the DDR mechanism is crucial for cancer treatment, and DDR-targeted drugs have been shown to be effective in different cancer types. This finding could provide potential benefits for use as a valuable tool for drug testing and understanding cholangiocarcinogenesis in a subset of CCAs.

Methods

Chemicals and reagents

Collagenase type IV, mouse monoclonal antibody against cytokeratin-7 (CK-7), and MTT reagent were purchased from Sigma–Aldrich (St. Louis, MO, USA). Mouse monoclonal antibody against cytokeratin-19 (CK-19) was obtained from Dako (Santa Clara, CA, USA). Ham's F12 nutrient mixture, MEM nonessential amino acids, fetal bovine serum (FBS), 0.25% trypan blue dye, and 0.25% trypsin–EDTA were purchased from Gibco BRL Life Technologies (Grand Island, NY, USA). The ROCK inhibitor was purchased from Santa Cruz Biotechnology (San Diego, CA, USA). Bovine serum albumin (BSA) was obtained from Capricorn Scientific (Hesse, Germany).

Patient background

Three donor patients were pathologically confirmed to have bile duct cancer. They were residents of the northeastern region of Thailand, in an area with liver fluke infections. Human samples were handled and processed under institutional guidelines and protocols approved by the Human Research Ethics Committee of Khon Kaen University (HE571283 and HE631599). The studies were conducted in accordance with the Declaration of Helsinki. All procedures were performed at Srinagarind Hospital, Faculty of Medicine, Khon Kaen University, Thailand, with informed written consent from patients. The primary tumor from a 53-year-old female with pCCA, encoded as H097 (later named KKU-097), a 62-year-old male with pCCA, encoded as 2KU140466 (KKU-466), and a 63-year-old female with iCCA, encoded as 2KU150610 (KKU-610), were obtained postsurgery. The patients were evaluated for serum AFP, CEA, and CA 19-9 tumor markers.

Establishment of human CCA cell lines

The CCA cells were derived from surgically resected liver specimens via protocols described in previous reports[11]. Briefly, tumor samples were processed under aseptic conditions by immersion in sterile Hank's balanced salt solution (HBSS) and subsequently minced into small fragments via scalpels. CCA tumor pieces were dissociated using 1 mg/ml collagenase type IV for 30–45 min at 37 °C. Then, the cell suspensions were washed with HBSS and resuspended in Ham's F12 nutrient mixture supplemented with 10% (v/v) FBS, 12.5 mM HEPES, MEM nonessential amino acids, an antibiotic mixture (50 µg/mL cefazolin, 10 µg/mL ciprofloxacin, and 2.5 µg/mL amphotericin B), and 5 µM ROCK inhibitor. The supernatant was then collected and filtered through a cell restrainer with a 70-mesh filter, followed by centrifugation at 2000 rpm for 5 min and culture in T25 cell culture flasks under an atmosphere of 5% CO_2 at 37 °C. The mixed fibroblasts were mechanically removed under a microscope during primary cell culture to purify the epithelial cells. Cultured cells were initially subpassaged every week until a stable growth rate was reached and then subpassaged when the cells reached 50–70% confluence using 0.25% trypsin–EDTA. Following a few passages of primary cultures, the ROCK inhibitor was removed from the medium mixture. The cell lines were tested for mycoplasma contamination via MycoAlert™ Plus Mycoplasma® (Lonza, Rockland, ME, USA) following the manufacturer's instructions.

Immunocytochemistry

CCA cells were cultured in a chamber with 2×10^4 cells/well for adherent growth. Following culture, the cells were rinsed twice with PBS, fixed with cold methanol for 20 min, and then air-dried before they were incubated with 5% BSA for 2 h. After that, the cells were incubated overnight with mouse monoclonal antibodies against CK-7 (1:500) and CK-19 (ready-to-use), followed by the secondary antibody of the standard horseradish peroxidase (HRP) method. The staining signal was assessed according to the intensity from no staining:

− = negative, + = < 25% tumor cells stained, + + = 25–50% tumor cells stained, and + + + = > 50% tumor cells stained.

Chromosome analysis

CCA cell lines were subjected to chromosome analysis upon achieving stability in culture. The established cells were treated with 1 µg/mL colcemid, followed by a hypotonic solution, and harvested according to standard cytogenetic procedures. The cells were fixed, dropped on slides, and subjected to trypsin–Giemsa banding to identify individual metaphase chromosomes. The representative chromosome was photographed for karyotype analysis with GenASIs Cytogenetics Suite Systems (Applied Spectral Imaging (ASI), Carlsbad, CA, USA). Three cytogeneticists (Y.C., M.T., and P.W.) analyzed the karyotypes of the CCA cells on the basis of the International System for Human Cytogenetic Nomenclature (ISCN) criteria[44].

Short tandem repeat analysis

DNA from CCA cells and original tissue was extracted using a genomic DNA extraction kit (Qiagen, Hilden, Germany). A standard STR profile was obtained with 23 loci and a sex marker (amelogenin). The obtained data were analyzed via GeneMapper™ ID-X software version 1.6 (Applied Biosystems, Waltham, MA, USA).

Morphological examination and growth kinetics

The cultured cells were regularly monitored and imaged via phase-contrast microscopy (Nikon Instruments, Tokyo, Japan). For population doubling time assessment, cells were seeded onto 6-well plates at a density of 1×10^4 cells, and the culture medium was changed every three days. The cells were detached from the wells with 0.25% trypsin–EDTA and stained with 0.25% trypan blue dye. The average number of viable cells was counted daily in a hemocytometer over 10 days. The growth curve was plotted, and the doubling time of the cell population was calculated during the log phase via the formula $Td = t \times Lg2/Lg(N1/N0)$, where Td is the doubling time, t is the time interval, N1 is the endpoint cell number, and N0 is the initial cell number.

Colony formation assay

CCA cells at a density of 600 cells/well were seeded in a 6-well plate and incubated overnight under 5% CO_2 at 37 °C for 14–21 days in complete medium, with medium renewal every three days. Then, the colonies of more than 50 cells were fixed with absolute methanol at 4 °C for 30 min, stained with 0.5% crystal violet in 2% ethanol for 1 h, washed with tap water to remove excess dye, and air-dried overnight. The colonies were captured via a ChemiDoc^{MP} imaging system (Bio-Rad, Hercules, CA, USA).

Wound healing assay

CCA cells at a density of 2×10^5 cells were seeded in a 24-well plate and allowed to adhere overnight. A wound was created in the cell monolayer by using a 200 µL sterile pipette tip, followed by washing with PBS to remove detached cells. The cells were then incubated in medium containing 10% FBS. Images of the wound gap were captured regularly until complete healing occurred. Cell migration, as measured by the closure of the wound gap, was analyzed via Image-Pro Plus software (Media Cybernetics Inc., Rockville, MD, USA).

Transwell migration and invasion assay

The migration assay was performed using a Transwell chamber (Corning, NY, USA). For the invasion assay, transwell chamber was briefly pre-coated with a 1:24 dilution of Matrigel solution (Corning, NY, USA) in coating buffer overnight. The excess gel was removed before 200 µL of cells (2×10^4 cells/well) in medium without 10% (v/v) FBS was seeded into the chamber. At the same time, 700 µL of medium supplemented with 10% (v/v) FBS was added to the lower chamber of the Transwell system. After incubation at 37 °C, the invading cells were fixed with absolute methanol for 30 min and stained with 0.5% crystal violet in 0.5% methanol for 10 min. Images of the invading cells were captured with a Nikon ECLIPSE Ni-U upright microscope (Nikon Instruments, Japan).

Drug sensitivity analysis

The chemotherapeutic sensitivity of CCA cells was evaluated by the MTT assay. Briefly, CCA cells were seeded onto 96-well plates at a density of 7.5×10^3 cells/well for KKU-466 and 5×10^3 cells/well for KKU-610 and KKU-097. After that, the cells were treated with various concentrations of Gem, Cis, or a combination for 24–72 h. For the assay, the plates containing treated cells were incubated with 100 µL of MTT in culture media without FBS (1:10 dilution) for 3 h. Following incubation, the formazan crystals were dissolved in dimethyl sulfoxide (DMSO). The absorbance was measured using a microplate reader at a wavelength of 540 nm.

Potential drug synergy in drug combinations was evaluated via SynergyFinder, a web application that uses a Bliss-independent model to quantify the degree of drug interaction. The synergy score is interpreted as the average excess response due to drug interactions, whereas scores of ≤ − 10, − 10 to 10, and ≥ 10 are likely to be antagonistic, additive and synergistic, respectively[45,46]. A 3D plot of the drug combination and Bliss score was created via SigmaPlot 10.0.

Whole exome sequencing and data analysis

WES was used to analyze gene mutations in 6 CCA cell lines. This analysis included KKU-097, KKU-466, KKU-610, and three previously established cell lines, including KKU-023 (JCRB1778), KKU-100 (JCRB1568), and KKU-452 (JCRB1772)[11,12]. DNA extraction from CCA cell lines was performed by using a QIAamp® blood mini kit (#51106, Qiagen, Hilden, Germany). Sequencing and data analysis were performed at Molecular Genomics (Molecular Genomics, Pte Ltd., Panda Loop, Singapore). Briefly, 100 ng of each DNA sample was quantified on a Qubit reader via a broad-range DNA assay kit (#Q32851, Thermo Fisher Scientific, USA). The assay libraries were

subsequently prepared via SureSelect XT HS v2 (Agilent, Santa Clara, CA, USA) following the manufacturer's protocol. The Human All Exon V8 SureSelect bait was used for capturing exonic regions. Libraries were sequenced on a NovaSeq 6000 platform with 2 × 150 bp paired-end sequences. The raw sequencing data (fastq files) were processed and analyzed using Agilent SureCall analysis software. The sequencing reads were aligned to the reference human genome (hg38). Variants were identified via SureCall's SNP caller with the following parameters: a variant score threshold of 0.3, minimum base quality of 30, variant call quality threshold of 100, and minimum allele frequency of 0.1. The criteria for selecting mutations included those that are clinically relevant, supported by evidence of pathogenicity, and related to the COSMIC, GWAS, and NCBI SNP databases. Furthermore, mutations were considered only if they included stop codons, exon deletions that maintained the reading frame, mutations in the start codon, missense mutations that occurred at stop codons, or insertions or deletions that caused a shift in the reading frame.

Four cell lines (KKU-023, KKU-097, KKU-452, and KKU-610) that matched tumor-adjacent normal tissue samples were available. Tissues were extracted from fresh frozen samples via the QIAamp® DNA Mini Kit (#51304, Qiagen, Hilden, Germany). The somatic mutations from paired tumor-normal tissues were examined via the Genome Analysis Toolkit (GATK) pipeline. The raw reads were aligned via BWA-0.7.1753[47]. The BAM files were generated through samtools-1.9 and then further processed through duplicate marking, base quality score recalibration, and variant quality score recalibration by GATK-4.1.0.054[48]. Somatic mutations were called by MuTect2 and annotated with ANNOVAR[49]. The resulting somatic variants were further filtered via GATK's FilterMutectCalls to retain high-confidence somatic mutations. Finally, the validated somatic mutations were functionally annotated for potential clinical actionability via databases such as OncoKB and classified on the basis of their likely impact on protein function and involvement in oncogenic pathways.

Sanger sequencing for TP53 and KRAS mutations

To investigate *TP53* and *KRAS* mutations in new CCA cell lines, KKU-100 was used as a positive control. Genomic DNA was extracted to analyze *KRAS* (NM_004985) mutations in exon 2. For the *TP53* (NM_000546) mutation, RNA was extracted from each cell line and subsequently converted to cDNA following the manufacturer's instructions (Bio-Rad Laboratories, Hercules, CA, USA). As previously reported, PCR amplification was performed using 100 ng of DNA template and specific PCR primer sequences for *TP53* and *KRAS*[11]. The quality of the PCR amplicons was assessed via agarose gel electrophoresis. For Sanger sequencing, the PCR products were purified via the Wizard® SV Gel and PCR Clean-Up System (Promega, Madison, WI, USA) and then subjected to nucleotide sequencing by the First BASE Laboratories (Selangor, Malaysia). Sequencing traces of the amplified products were aligned to reference sequences via Lasergene 10.1 (DNASTAR) and analyzed via visual inspection.

Comparison of mutational spectra in CCA cells

Principal component analysis (PCA) was used to examine differential mutational patterns among CCA cell lines. The analysis was performed via Python (version 3.12.3) with the sklearn.decomposition package. The mutational data from 10 CCA cells (KKU-097, KKU-466, KKU-610, KKU-023, KKU-452 cells, KKU-100, KKU-055, KKU-213A, KKU-213B, and KKU-213C cells) were encoded in a binary format, with mutations represented as '1' and nonmutations as '0'. This method was implemented to reduce the degree of technical variability among different WES platforms and ensure consistent data analysis across samples.

Data availability

Sequence data that support the findings of this study have been deposited in the NCBI's SRA database with the primary accession code PRJNA1144247.

Received: 5 August 2024; Accepted: 5 March 2025
Published online: 13 March 2025

References

1. Byrling, J., Andersson, B., Andersson, R. & Marko-Varga, G. Cholangiocarcinoma—Current classification and challenges towards personalised medicine. *Scand. J. Gastroenterol.* **51**, 641–643. https://doi.org/10.3109/00365521.2015.1127409 (2016).
2. Banales, J. M. et al. Cholangiocarcinoma 2020: The next horizon in mechanisms and management. *Nat. Rev. Gastroenterol. Hepatol.* **17**, 557–588. https://doi.org/10.1038/s41575-020-0310-z (2020).
3. Sripa, B. & Pairojkul, C. Cholangiocarcinoma: Lessons from Thailand. *Curr. Opin. Gastroenterol.* **24**, 349–356. https://doi.org/10.1097/MOG.0b013e3282fbf9b3 (2008).
4. Khan, S. A., Tavolari, S. & Brandi, G. Cholangiocarcinoma: Epidemiology and risk factors. *Liver Int.* **39**(Suppl 1), 19–31. https://doi.org/10.1111/liv.14095 (2019).
5. Kirstein, M. M. & Vogel, A. Epidemiology and risk factors of cholangiocarcinoma. *Visc. Med.* **32**, 395–400. https://doi.org/10.1159/000453013 (2016).
6. Banales, J. M. et al. Expert consensus document: Cholangiocarcinoma: Current knowledge and future perspectives consensus statement from the European Network for the Study of Cholangiocarcinoma (ENS-CCA). *Nat. Rev. Gastroenterol. Hepatol.* **13**, 261–280. https://doi.org/10.1038/nrgastro.2016.51 (2016).
7. Chan-On, W. et al. Exome sequencing identifies distinct mutational patterns in liver fluke-related and non-infection-related bile duct cancers. *Nat. Genet.* **45**, 1474–1478. https://doi.org/10.1038/ng.2806 (2013).
8. Jusakul, A. et al. Whole-genome and epigenomic landscapes of etiologically distinct subtypes of cholangiocarcinoma. *Cancer Discov.* **7**, 1116–1135. https://doi.org/10.1158/2159-8290.CD-17-0368 (2017).
9. Jusakul, A., Kongpetch, S. & Teh, B. T. Genetics of opisthorchis viverrini-related cholangiocarcinoma. *Curr. Opin. Gastroenterol.* **31**, 258–263. https://doi.org/10.1097/MOG.0000000000000162 (2015).
10. Isidan, A. et al. Development and characterization of human primary cholangiocarcinoma cell lines. *Am. J. Pathol.* **192**, 1200–1217. https://doi.org/10.1016/j.ajpath.2022.05.007 (2022).

11. Saensa-Ard, S. et al. Establishment of cholangiocarcinoma cell lines from patients in the endemic area of liver fluke infection in Thailand. *Tumour Biol.* **39**, 1010428317725925. https://doi.org/10.1177/1010428317725925 (2017).
12. Sripa, B. et al. Establishment and characterization of an opisthorchiasis-associated cholangiocarcinoma cell line (KKU-100). *World J. Gastroenterol.* **11**, 3392–3397. https://doi.org/10.3748/wjg.v11.i22.3392 (2005).
13. Sripa, B. et al. Functional and genetic characterization of three cell lines derived from a single tumor of an Opisthorchis viverrini-associated cholangiocarcinoma patient. *Hum. Cell.* **33**, 695–708. https://doi.org/10.1007/s13577-020-00334-w (2020).
14. Brindley, P. J. et al. Cholangiocarcinoma. *Nat. Rev. Dis. Primers* **7**, 65. https://doi.org/10.1038/s41572-021-00300-2 (2021).
15. Li, Y., Song, Y. & Liu, S. The new insight of treatment in Cholangiocarcinoma. *J. Cancer* **13**, 450–464. https://doi.org/10.7150/jca.68264 (2022).
16. Ong, C. K. et al. Exome sequencing of liver fluke-associated cholangiocarcinoma. *Nat. Genet.* **44**, 690–693. https://doi.org/10.1038/ng.2273 (2012).
17. Lee, J. H. & Lee, S. W. The roles of carcinoembryonic antigen in liver metastasis and therapeutic approaches. *Gastroenterol. Res. Pract.* **2017**, 7521987. https://doi.org/10.1155/2017/7521987 (2017).
18. Zhao, H. & Lu, B. Prediction of multiple serum tumor markers in hepatolithiasis complicated with intrahepatic cholangiocarcinoma. *Cancer Manag. Res.* **14**, 249–255. https://doi.org/10.2147/CMAR.S344711 (2022).
19. Eschrich, J. et al. The diagnostic approach towards combined hepatocellular-cholangiocarcinoma-state of the art and future perspectives. *Cancers (Basel)* https://doi.org/10.3390/cancers15010301 (2023).
20. Vainshelbaum, N. M., Zayakin, P., Kleina, R., Giuliani, A. & Erenpreisa, J. Meta-analysis of cancer triploidy: Rearrangements of genome complements in male human tumors are characterized by XXY karyotypes. *Genes (Basel)* https://doi.org/10.3390/genes10080613 (2019).
21. Gerashchenko, B. I. et al. Disentangling the aneuploidy and senescence paradoxes: A study of triploid breast cancers non-responsive to neoadjuvant therapy. *Histochem. Cell. Biol.* **145**, 497–508. https://doi.org/10.1007/s00418-016-1415-x (2016).
22. Suhail, Y. et al. Systems biology of cancer metastasis. *Cell Syst.* **9**, 109–127. https://doi.org/10.1016/j.cels.2019.07.003 (2019).
23. Fares, J., Fares, M. Y., Khachfe, H. H., Salhab, H. A. & Fares, Y. Molecular principles of metastasis: A hallmark of cancer revisited. *Signal Transduct. Target Ther.* **5**, 28. https://doi.org/10.1038/s41392-020-0134-x (2020).
24. Aslam, A., Wasnik, A. P., Shi, J., Sahai, V. & Mendiratta-Lala, M. Intraductal papillary neoplasm of the bile duct (IPNB): CT and MRI appearance with radiology-pathology correlation. *Clin. Imaging* **66**, 10–17. https://doi.org/10.1016/j.clinimag.2020.04.036 (2020).
25. Wan, X. S. et al. Intraductal papillary neoplasm of the bile duct. *World J. Gastroenterol.* **19**, 8595–8604. https://doi.org/10.3748/wjg.v19.i46.8595 (2013).
26. Panawan, O. et al. Establishment and characterization of a novel cancer stem-like cell of cholangiocarcinoma. *Cancer Sci.* **114**, 3230–3246. https://doi.org/10.1111/cas.15812 (2023).
27. Miao, X. et al. Establishment and characterization of a new intrahepatic cholangiocarcinoma cell line derived from a Chinese patient. *Cancer Cell Int.* **22**, 418. https://doi.org/10.1186/s12935-022-02840-3 (2022).
28. Xu, H. et al. Establishment and characterization of a new intrahepatic cholangiocarcinoma cell line, ICC-X2. *World J. Oncol.* **15**, 114–125. https://doi.org/10.14740/wjon1757 (2024).
29. Zheng, Q., Zhang, B., Li, C. & Zhang, X. Overcome drug resistance in cholangiocarcinoma: New insight into mechanisms and refining the preclinical experiment models. *Front. Oncol.* **12**, 850732. https://doi.org/10.3389/fonc.2022.850732 (2022).
30. Jiang, T. Y. et al. PTEN deficiency facilitates gemcitabine efficacy in cancer by modulating the phosphorylation of PP2Ac and DCK. *Sci. Transl. Med.* **15**, eadd7464. https://doi.org/10.1126/scitranslmed.add7464 (2023).
31. Lee, S. H. et al. ARID1A mutation from targeted next-generation sequencing predicts primary resistance to gemcitabine and cisplatin chemotherapy in advanced biliary tract cancer. *Cancer Res. Treat.* **55**, 1291–1302. https://doi.org/10.4143/crt.2022.1450 (2023).
32. Parasramka, M. et al. BAP1 dependent expression of long non-coding RNA NEAT-1 contributes to sensitivity to gemcitabine in cholangiocarcinoma. *Mol. Cancer* **16**, 22. https://doi.org/10.1186/s12943-017-0587-x (2017).
33. Jones, S. et al. Somatic mutations in the chromatin remodeling gene ARID1A occur in several tumor types. *Hum. Mutat.* **33**, 100–103. https://doi.org/10.1002/humu.21633 (2012).
34. Zang, Z. J. et al. Exome sequencing of gastric adenocarcinoma identifies recurrent somatic mutations in cell adhesion and chromatin remodeling genes. *Nat. Genet.* **44**, 570–574. https://doi.org/10.1038/ng.2246 (2012).
35. Lu, S., Duan, R., Cong, L. & Song, Y. The effects of ARID1A mutation in gastric cancer and its significance for treatment. *Cancer Cell. Int.* **23**, 296. https://doi.org/10.1186/s12935-023-03154-8 (2023).
36. Kim, D. et al. Pan-KRAS inhibitor disables oncogenic signalling and tumour growth. *Nature* **619**, 160–166. https://doi.org/10.1038/s41586-023-06123-3 (2023).
37. Janne, P. A. et al. Adagrasib in non-small-cell lung cancer harboring a KRAS(G12C) mutation. *N. Engl. J. Med.* **387**, 120–131. https://doi.org/10.1056/NEJMoa2204619 (2022).
38. Skoulidis, F. et al. Sotorasib for Lung Cancers with KRAS p.G12C Mutation. *N. Engl. J. Med.* **384**, 2371–2381. https://doi.org/10.1056/NEJMoa2103695 (2021).
39. Tria, S. M., Burge, M. E. & Whitehall, V. L. J. The therapeutic landscape for KRAS-mutated colorectal cancers. *Cancers (Basel)* https://doi.org/10.3390/cancers15082375 (2023).
40. Gorodetska, I., Kozeretska, I. & Dubrovska, A. BRCA genes: The Role in genome stability, cancer stemness and therapy resistance. *J. Cancer* **10**, 2109–2127. https://doi.org/10.7150/jca.30410 (2019).
41. O'Connor, M. J. Targeting the DNA damage response in cancer. *Mol. Cell* **60**, 547–560. https://doi.org/10.1016/j.molcel.2015.10.040 (2015).
42. Lord, C. J. & Ashworth, A. PARP inhibitors: Synthetic lethality in the clinic. *Science* **355**, 1152–1158. https://doi.org/10.1126/science.aam7344 (2017).
43. Peng, J. et al. Genetic alterations of KRAS and TP53 in intrahepatic cholangiocarcinoma associated with poor prognosis. *Open Life Sci.* **18**, 20220652. https://doi.org/10.1515/biol-2022-0652 (2023).
44. McGowan-Jordan, J., Hastings, R. J. & Moore, S. A. *ISCN 2020: An International System for Human Cytogenomic Nomenclature* (Karger Medical and Scientific Publishers, 2020).
45. Mahaamnad, N. et al. Dual blockage of PI3K-mTOR and FGFR induced autophagic cell death in cholangiocarcinoma cells. *Heliyon* **10**, e31112. https://doi.org/10.1016/j.heliyon.2024.e31112 (2024).
46. Zheng, S. et al. SynergyFinder Plus: Toward better interpretation and annotation of drug combination screening datasets. *Genom. Proteomics Bioinf.* **20**, 587–596. https://doi.org/10.1016/j.gpb.2022.01.004 (2022).
47. Li, H. & Durbin, R. Fast and accurate short read alignment with Burrows-Wheeler transform. *Bioinformatics* **25**, 1754–1760. https://doi.org/10.1093/bioinformatics/btp324 (2009).
48. McKenna, A. et al. The genome analysis toolkit: a MapReduce framework for analyzing next-generation DNA sequencing data. *Genome Res.* **20**, 1297–1303. https://doi.org/10.1101/gr.107524.110 (2010).
49. Wang, K., Li, M. & Hakonarson, H. ANNOVAR: Functional annotation of genetic variants from high-throughput sequencing data. *Nucleic Acids Res.* **38**, e164. https://doi.org/10.1093/nar/gkq603 (2010).

Author contributions

R.J. performed the experiments, analyzed data, and wrote the manuscript. A.J. designed the study, analyzed data and wrote the manuscript. P.P. designed the study and performed a comparison of mutational spectra analysis. V.K. wrote, reviewed, and revised the manuscript. L.S. and A.P. provided material and technical support. W.L. and N.N. provided patient samples. A.T., Ap.J., V.T., and N.K. contributed to clinical diagnosis and sample collection. Y.C., M.T., and P.W. performed karyotypes analysis. J.H.H., P.G., and H.L.H. performed WES analysis. C.P. performed histological diagnosis and provided material specimens. B.T.T. provided WES analysis and suggestions. S.K. conceived, designed, supervised the research, wrote and revised the manuscript. All authors have read and approved the final manuscript.

Funding

S.K. was supported by NSRF under the Basic Research Fund of Khon Kaen University and the Faculty of Medicine, Khon Kaen University, Thailand (Grant Number IN67050). R.J. was supported by Research Fund for Supporting Lecturer to Admit High Potential Student to Study and Research on His Expert Program Year 2022, Graduate School, Khon Kaen University (651H220). B.T.T., P.G., and J.H.H. were supported by the 3rd A*STAR-AMED Joint Grant (R23I2IR070). B.T.T. was supported by the National Medical Research Council Singapore Translational Research Investigator Award (NMRC MOH-000248-00), the Tan Yew Oo Professorship in Pathology, the Verdant Foundation, and the NCC Cancer Fund.

Declarations

Competing interests

The authors declare no competing interests.

Additional information

Supplementary Information The online version contains supplementary material available at https://doi.org/10.1038/s41598-025-93192-1.

Correspondence and requests for materials should be addressed to S.K.

Reprints and permissions information is available at www.nature.com/reprints.

Publisher's note Springer Nature remains neutral with regard to jurisdictional claims in published maps and institutional affiliations.